

Computer Aided Prostate Cancer Diagnosis Using Image Enhancement and JPEG2000

Ming Gao^a, Phillip Bridgman^b and Sunil Kumar^{a*}

^aElectrical and Computer Engineering, Clarkson University, Potsdam, NY 13699, USA

^bPathology Lab, Canton Potsdam Hospital, Potsdam, NY 13676, USA

ABSTRACT

This paper introduces the applications of image processing and JPEG2000 in pathology. Our study aims to provide pathologists valuable assistance on examining biopsy samples of prostate and support their decision. The digital color microscopic image is processed only within the regions of interest instead of overall processing. In this way, some diagnostic information is enhanced to provide better visual effect. JPEG2000 is used for the storage and interactive transmission of the large pathological images. Our simulation results show that the use of JPEG2000 can significantly save storage space without compromising the diagnostic value of the image.

Keywords: Prostate cancer diagnosis, image enhancement, JPEG2000, color space, pathology, image processing.

1. INTRODUCTION

Cancer ranks as the second largest killer of Americans¹. The incidence of prostate cancer is increasing rapidly, and almost one-third of American men over 50 years old will be diagnosed with prostate cancer during their life times. Therefore, urologists suggest men have a prostate examination by the age of 50. Generally, the examinations begin with a Prostate Specific Antigen (PSA) test². The patient is recommended to have a core biopsy if a urologist finds a PSA level higher than a normal value. Usually, the biopsy procedure is performed with biopsy guns based on certain positioning protocols. Then an experienced pathologist will examine the tissue samples under a microscope to determine whether there is prostate gland cancer based on biological features. If cancer is found, the pathologist should also grade the cancer using an accepted grading scheme, such as Gleason or Mostofi. In America, the Gleason grading system is the most commonly used grading scheme³. It is a five level scoring system strictly based on the organization features of prostatic glands. The ability of a tumor to mimic normal gland architecture is called its differentiation. Low grade of tumor means its structure is very well differentiated, but high grade means that the tumor is poorly differentiated and is aggressively malignant. For instance, grades 1 and 2 are composed of more uniform and closely packed glands. Grade 3 tumors have glands, which vary in size and shape more than those in grades 1 and 2, and the glands in grade 3 are described as having an "invasive" appearance. Grade 3 glands also tend to be more randomly distributed and more widely separated than grades 1 and 2. Grade 4 is assigned to a tumor when the pattern of individual, separate gland units is almost entirely lost. In grade 5 tumors, it is difficult to find evidence of gland unit and only a sea of nuclei is visible. The Gleason system is regarded as the most useful method for grading prostate cancer by urologists, oncologists and pathologists and has a great influence on treatment planning⁴. Since the grading process is performed manually by human beings (i.e., pathologists), it is affected by "inter- and intra-observer variations"¹. As a result, the grading process is partially subjective. Studies have revealed a 20% discrepancy in combined Gleason score (the sum of the two most prominent grades in prostate adenocarcinoma) assigned by the practicing pathologists⁴.

Therefore, there is a need to develop computer-aided diagnostic tools (e.g., using image processing techniques) for the purpose of more accurate and efficient diagnosis and prognosis⁴⁻¹⁵. However, very little work has been done in applying such techniques to histology, due to the complexity of histopathological images. Nuclear roundness factor (NRF) analysis was proposed for predicting the behavior of low-stage cancers⁵. However, the requirement for manual

* skumar@clarkson.edu; phone 315-268-6602; fax 315-268-7600

nuclear contour tracing makes this method tedious and slow. An early work by Kim *et al*⁶, using semi-automated analysis of NRF, automatically detected nuclear boundaries by using a multiscale segmentation algorithm and discriminated artifacts in a semi-automated way. But NRF analysis cannot be applied to cancers of any grade because the monotonic relationship of NRF and grade is lost in high grade cancer⁵. Roula *et al*⁸ applied multispectral imaging in the analysis of pathological tissues and obtained additional spectral data for classification of prostate samples. Pitts *et al*⁹ investigated the application of gray level co-occurrence matrix techniques for the interpretation of prostate cancer lesions and identifying corresponding features on the color images of the section. Bartels *et al*¹⁰⁻¹⁴ built a machine vision system which was for automated detection of regions of abnormality, image object segmentation, diagnostic information extraction, and diagnostic evidence evaluation.

However, the following factors might affect the grading: very small sample size, invisible part, poorly cut sections, poor quality staining, obscuring inflammation, and atypical or atrophic glands. Therefore, the microscopic image should be adjusted to gain better visual effect. Before grading the cancer, a pathologist must distinguish benign from malignant glands according to certain diagnostic clues, e.g. number of cell layers of a gland (single or multiple layers), number of cells in a gland, size of nuclei and nucleoli, the ratio of nucleus size to cytoplasm size. Bartels *et al* found methods to segment basal cells and calculate the ratio of number of gaps in the basal cell layer to layer perimeter length. In order to have a better segmentation, besides using conventional stains, they also used cytokeratin marker 34 β E12 to stain the basal cells with distinctive optical density, i.e. yellow brown tone, and other part with red tone^{12,13,14}. Since they used a special stain to segment the object, it may not apply to other conventionally stained images, used by practicing pathologists. The ray tracing method¹⁴ is probably restricted to the image that includes only one gland.

Since most practicing pathologists examine the specimen using a light microscope, they have to depend only on the locally available case material for comparison in difficult cases. The dissemination of case material for consultative, investigative or educational purposes is quite laborious at present. Computer-aided analysis cannot only help pathologists perform a better visual examination of specimen but also allow them the access to a database of pre-graded samples for comparison. Wetzel *et al*^{4,7} built a database containing plenty of accurately graded tissue images, and developed a content-based image retrieval system to assist pathologists by comparing image features of undiagnosed samples with the pre-graded images stored in the database. Over the past decade, there has also been increasing interest in technologies in the areas of telepathological imaging that enables the examination of a pathological specimen at a distance¹⁵. Apart from imaging processing tools, the computer-aided analysis also requires efficient storage and transmission facilities for images. For example, a 2048 \times 1536, 24 bit RGB color image of a biopsy specimen slide requires about 9.5 MB memory space. Clearly there is an enormous storage requirement as the hospitals can generate thousands of slides each year. This calls for the use of sophisticated compression techniques equipped with useful features, to reduce the storage space in databases without compromising diagnostic quality of the images.

In this paper, we first discuss two enhancement schemes for enhancing the details pertaining to cell regions (i.e., nuclei and cytoplasm). This is followed by JPEG2000-based compression studies to find out the acceptable compression ratios and corresponding peak signal-to-noise ratios (PSNRs). The remaining paper is organized as follows. In Section 2, we discuss our proposed scheme, consisting of image enhancement and compression modules. The simulation results and discussion are presented in Section 3. The conclusions are given in the Section 4.

2. THE PROPOSED SCHEME

In this section we shall first discuss our image enhancement schemes, followed by JPEG2000-based compression scheme for the original as well as enhanced images.

2.1 Image Acquisition:

Prostate needle biopsies were taken from men with elevated serum PSA levels, or abnormal nodules discovered on digital rectal examination. Six to eight tissue cores were fixed in 10% neutral buffered formalin. All biopsies were routinely embedded in paraffin and were cut at a thickness of 5 um. The tissue sections on the slides were stained with hematoxylin and eosin. The images were taken using a Nikon bright field microscope with a Nikon Coolpix 990 digital camera. The photographs were taken at a magnification of 400X, and were saved in TIFF format using 24 bpp.

2.2 Image enhancement schemes:

Microscopic views of histological tissues show structures mostly arranged in a variety of patterns. Therefore, the automatic segmentation of different structures, like cells, nuclei, cytoplasm, vessels, etc. is difficult. The practical applicability of the analysis of histological tissues is thus largely limited by the problem of detecting structures of interest. The prostate gland image includes glands and stroma. A gland is made up of cells and a lumina. From the microscopic image, it is possible to observe the nucleus and cytoplasm regions of a cell. In our scheme, an application with a friendly interface is designed for analyzing the whole image. Since a pathologist is more concerned with the cell region of gland, our image enhancement schemes concentrate mainly on the two parts: nuclei and cytoplasm. We call the enhancement schemes as '*nuclei enhancement*' and '*cytoplasm enhancement*', respectively. By comparing the enhanced image with the original image, the pathologist can find some of the invisible information becoming clearer. For instance, a visible nucleolus means that the cell is probably an abnormal cell, but in an original image it may not be possible to find detailed information about some nuclei because of poor contrast in the luminance as well as chrominance components in the nuclei regions. In the corresponding enhanced image, more nucleoli may become visible. Such cells may be of higher interest to the pathologist.

Since RGB is not an appropriate model for segmenting colors based on color sensing properties of human visual system, we have chosen HSI color model for this purpose. In HSI color space, hue (H) and saturation (S) determine the chromatic information while intensity (I) represents the brightness.

First, we convert RGB color space image to HSI space beginning with normalizing RGB values:

$$r = \frac{R}{R+G+B}, g = \frac{G}{R+G+B}, b = \frac{B}{R+G+B}.$$

Each normalized H, S and I components are then obtained by¹⁶,

$$h = \cos^{-1} \left\{ \frac{0.5 \cdot [(r-g) + (r-b)]}{(r-g)^2 + (r-b)(g-b)^{1/2}} \right\} \quad h \in [0, \pi] \text{ for } b \leq g$$

$$h = 2\pi - \cos^{-1} \left\{ \frac{0.5 \cdot [(r-g) + (r-b)]}{(r-g)^2 + (r-b)(g-b)^{1/2}} \right\} \quad h \in [0, \pi] \text{ for } b > g$$

$$s = 1 - 3 \cdot \min(r, g, b) \quad s \in [0, 1]$$

$$i = (r + g + b) / 3 \quad i \in [0, 1].$$

For convenience, h, s and i values are converted in the ranges of [0,360], [0,100], [0, 255], respectively by:

$$H = h \times 180 / \pi; S = s \times 100 \text{ and } I = i \times 255.$$

Nuclei Enhancement: By inspecting and comparing each region in test images, we have heuristically found that nuclei have H, S and I values in the ranges of [300,335], (45,100] and (82, 200), respectively. In order to enhance the contrast of nuclei, the following scaling function is used on intensity component:

$$I' = \begin{cases} \frac{b_1}{a_1} I & I \in [0, a_1] \\ \frac{b_2 - b_1}{a_2 - a_1} (I - a_1) + b_1 & I \in (a_1, a_2] \\ \frac{255 - b_2}{255 - a_2} (I - a_2) + b_2 & I \in (a_2, 255] \end{cases} \dots (1)$$

where I is original intensity value; I' is its new intensity value; values of a_1, a_2, b_1 and b_2 can be chosen experimentally. Figure 2 shows the contrast enhancement function.

Cytoplasm Enhancement: Similarly, we have observed that the values of H, S and I in the cell regions (excluding stroma and lumina regions) lie in the ranges of [280,338], (3,100] and [0,221), respectively. The regions of cytoplasm and cell membrane can be obtained by removing nuclei from these regions. Using the test images, we have experimentally determined that the H, S and I values given by union of the following five conditions given in Table 1 correspond to regions of cytoplasm and cell membrane:

Table 1: HSI features of cytoplasm and cell membrane regions

	Hue	Saturation	Intensity
1	[280,300]	[3,100]	[0,221]
2	[335,338]	[3,100]	[0,221]
3	[280,338]	[3,45]	[0,221]
4	[280,338]	[3,100]	[0,82]
5	[280,338]	[3,100]	[200,221]

In order to enhance the contrast of cytoplasm and cell membrane, a scaling function as given in equation 1 is used on S component of corresponding regions.

Finally, the image processed in HSI color space should be transformed back to RGB color space for storing and displaying. The inverse transform is given as:

$$h = H \cdot 180 / \pi; s = S / 100; i = I / 255$$

$$x = i \cdot (1 - s)$$

$$y = i \cdot \left[1 + \frac{s \cdot \cos(h)}{\cos(\pi/3 - h)} \right]$$

$$z = 3i - (x + y);$$

when $h < 2\pi/3$, $b = x$; $r = y$ and $g = z$.

when $2\pi/3 \leq h < 4\pi/3$, $h = h - 2\pi/3$, and $r = x$; $g = y$ and $b = z$.

when $4\pi/3 \leq h < 2\pi$, $h = h - 4\pi/3$, and $g = x$; $b = y$ and $r = z$.

The resulting r, g and b are normalized values in the ranges of [0,1]; they are multiplied by 255 for displaying.

2.3 JPEG2000-based compression:

Usually, a pathological digital image has high resolution, which results in large size of the image file as explained in Section I. Storing huge amount of image files and transmitting such large files however pose practical problems. Medical image storage and transmission systems, commonly known as PACS (or picture archiving and transmission systems) are expected to use wavelet-based compression for efficient storage and transmission of the massive volumes of the medical imaging data. JPEG2000, with many useful features, can be an ideal solution for this¹⁷⁻¹⁹. This latest image compression standard is based on wavelet decomposition and provides higher compression ratio than other still

image compression standards, such as JPEG, MPEG-4 VTC¹⁸⁻¹⁹. JPEG2000 supports lossless, visually lossless as well as lossy compression in a unified framework. It offers PSNR scalability (in addition to several other types of scalabilities) so that a single compressed data stream can be decompressed at many bit-rates. Similarly, the spatial scalability feature allows an image to be reconstructed at different resolutions, in terms of image size such as half or quarter the size of original image. Therefore, many images of different perceptual quality can be obtained from only one compressed bitstream. The medical images are not supposed to be compressed in a lossy manner. However, wavelet-based compression schemes are finding increasing acceptance in the medical community. The degree to which images can be compressed and still maintain diagnostic integrity is unknown. The JPEG2000 standard also supports 'region of interest (ROI)' coding feature, by which some of the image regions that are of critical value to the image diagnosis can be reconstructed at a higher quality than rest of the image, depending on the user's interest. We have tried to find out how much compression ratio can be obtained without compromising the diagnostic value of the image. Since our image processing module suggests the use of contrast enhancements in cell regions, the reconstructed image should be of excellent diagnostic quality in the normal as well as enhanced format. Figure 1 shows the block diagram (or flow chart) of the whole procedure of our computer aided diagnosis scheme. Ideally, the image can be compressed and stored in a database, at a high enough bit-rate using JPEG2000 so that it is visually lossless for diagnostic purposes. A pathologist can retrieve the compressed image data interactively till acceptable quality image at a desired size is reconstructed.

3. SIMULATION RESULTS AND DISCUSSION

Fig. 3 shows a typical microscopic image of a biopsy sample of a section of prostate gland. The test images are 2048×1536 , 24 bit RGB color images. Fig. 4 shows segmented nuclei region of Fig. 3 by selecting appropriate H, S, and I values in the range of [300,335], (45,100] and (82, 200), respectively, such that the background region appears dark and the appearance of nuclei region remains unchanged. We find that there is no single rule for any one of the three components in HSI color space to segment the region shown in Fig. 4; this is why we have used a combination of 3 values. Since image in Fig. 3 is too big to fit the computer screen, an upper-left portion of Fig. 3 is shown in Fig 5 at full resolution. As explained in previous section, a cell's nucleus and its nucleolus play major role in the image diagnosis. However, it is not possible to identify them separately in many cells in Fig. 3 or 5 with naked eyes, because of the minor intensity difference within each nucleus. Therefore, we have done '*nuclei enhancement*' to adjust the contrast of the nuclei region by using equation (1) on the intensity component in HSI color space, where $a_1 = 82$, $a_2 = 125$, $b_1 = 70$ and $b_2 = 200$. Here $[a_1, a_2]$ represents the range of I component in the original HSI color space image that is altered in enhancement process to the range represented by $[b_1, b_2]$. Fig. 6 is the enhanced image of the same portion, where the intensity of only the nuclei regions is enhanced while the intensity of other regions remains unchanged. Comparing Figs. 5 and 6, we can see that several nucleoli have become more visible or clearer in Fig. 6. Those cells whose nucleoli are visible may probably be of more interest to pathologist because they are likely to be diagnosed as malignant cells.

The size of the nucleus in each cell provides additional important information, but many cells appear to be merged together or overlapped so that they cannot be identified separately. Based on combinations of HSI values given in Table 1, the regions of cytoplasm and membrane of Fig. 3 are segmented as shown in Fig. 7. We have done '*cytoplasm enhancement*' to make membrane color more pure by using equation (1) on the Saturation component in HSI color space, where $a_1 = 29$, $a_2 = 30$, $b_1 = 27$ and $b_2 = 35$. A lower-left portion of Fig. 3 is shown in Fig. 8. Fig. 9 is the enhanced image of the same portion, and we can see that membrane's color is strengthened to some extent.

We choose three test images to study the peak signal-to-noise ratios (PSNRs) at different bit-rates after JPEG2000-based compression. Our goal is to find out how much compression can be obtained without compromising the diagnostic integrity of the image. We have used the JPEG2000 codec provided by Kakadu Version 2.2 (University of New South Wales, Sydney, Australia). We set the encoding parameters as Creversible=yes, Cycc=yes, Clayers=50, rate=24, with PSNR and spatial scalability enabled. Enhancements have been done both on the original and reconstructed images. Then, we compare each pair of two corresponding images. The PSNR values for each of RGB

component are shown in Table 2 for a representative test image. The plot of these values is shown in Fig. 10. Similar values have been obtained for other test images. In order to have better understanding of the above results, we show a difference image in Fig. 11, at 2 bpp. This gives us a compression ratio of 12, as each pixel in the original color image is represented using 24 bits. Each pixel in the difference image is magnified 100 times to obtain good visual effect. Medians and standard deviations of the pixel value differences for the original and reconstructed test image are shown in Table 3. The reconstructed images at different bit-rates were subjectively examined by the pathologist, to check the loss of useful information (i.e., diagnostic integrity). Our experimental results show that the loss of image fidelity is minimal up to a bit rate of 2 bpp. For a 2048x1536, RGB image at 24 bpp this requires 9.5 MB memory space, resulting in a saving of about 8.6 Mbytes. Please note that the image can be compressed losslessly at about 9 bpp, which corresponds to a compression ratio of 2.5:1.

Table 2: PSNR values of the compressed test image at different bit-rates

PSNR (dB)	No enhancement	Nuclei enhancement	Cytoplasm enhancement
Bitrate (bpp)	R/G/B	R/G/B	R/G/B
0.5	39.5/38.6/37.1	35.2/34.4/29.4	37.6/36.2/36.8
1	40.5/40.0/38.8	35.9/35.3/30.3	38.4/37.3/38.5
2	42.6/42.5/41.1	37.4/36.9/31.7	40.3/39.5/40.6
5	46.5/47.4/44.1	40.4/39.5/33.9	43.5/43.1/43.3
8	52.9/55.0/50.8	44.7/43.9/38.1	48.0/48.3/48.6

Table 3: Mean and Standard Deviation of pixel values differences in test image No.1

		No enhancement	Nuclei enhancement	Cytoplasm enhancement
Bitrate (bpp)		R/G/B	R/G/B	R/G/B
1	Mean	1.81/1.91/2.27	1.90/2.41/3.23	2.05/2.28/2.35
	Std Dev	1.61/1.69/1.88	3.67/3.66/7.17	2.28/2.60/1.92
2	Mean	1.40/1.43/1.73	1.49/1.81/2.48	1.61/1.73/1.83
	Std Dev	1.26/1.28/1.45	3.14/3.16/6.14	1.88/2.09/1.51
8	Mean	0.31/0.21/0.46	0.46/0.31/0.75	0.49/0.32/0.58
	Std Dev	0.49/0.42/0.59	1.42/1.62/3.08	0.89/0.94/0.76

4. CONCLUSION

We developed methods and an application for applying image processing and JPEG2000 principles to help pathologists derive more information from the image. The RGB color image was transformed into HSI color space in which the color and intensity can be adjusted independently. In this way we have had good initial results. In decompression part, each image is reconstructed at different bitrate to test the visual difference from the original one and to calculate PSNR and other statistical values. Our test results showed that the image reconstructed at lower bitrate has only minor visual difference with the images reconstructed at higher bitrate. This study demonstrates that low bitrate JPEG2000 image can be used for pathological diagnostic studies of prostate cancer.

REFERENCES

1. V. Kumar, R. Cotran, S.L. Robbins, *Basic Pathology*, W.B. Saunders Company, 1997.
2. D.G. Bostwick, J.N. Eble, *Urologic Surgical Pathology*, Mosby – year book, inc. 1997.
3. D.F. Gleason, G.T. Mellinger, *et al*, “Prediction of prognosis for prostatic adenocarcinoma by combined histological grading and clinical staging”, *Journal of Urology*, **111**, 58-64, 1974.
4. A.W. Wetzel, R. Crowley, S.J. Kim, R. Dawson, L. Zheng, Y.M. Joo, Y. Yagi, J. Gilbertson, C. Gadd, D.W. Deerfield, M.J. Becich, “Evaluation of prostate tumor grades by content based image retrieval”, 27th AIPR

- Workshop: Advances in Computer Assisted Recognition, Washington D.C., Oct. 16, 1998, SPIE Proceedings, 3584, pp. 244-252.
5. T.D. Clark, F.B. Askin, C.R. Bagnell, "Nuclear Roundness Factor: A Quantitative Approach To Grading In Prostate Carcinoma, Reliability Of Needle Biopsy Tissue, And The Effect Of Tumour Stage On Usefulness", *The Prostate*, **10**, 199-206, 1987.
 6. D. Kim, J.D. Charlton, J.M. Coggins, J.L. Mohler, "Semiautomated nuclear shape analysis of prostatic carcinoma and benign prostatic hyperplasia", *Analytical Quantitative Cytology and Histology*, **16(6)**, 400-414, 1994.
 7. A.W. Wetzel, "Computational Aspects of Pathology Image Classification and Retrieval", *Journal of Supercomputing*, **11**, 279-93, 1997.
 8. M.A. Roula, J. Diamond, A. Bouridane, P. Miller and A. Amira, "A Multispectral Computer Vision System For Automatic Grading Of Prostatic Neoplasia", Proceedings of IEEE International Symposium on Biomedical Imaging, 2002.
 9. D.E. Pitts, B.S. Premkumar, A.G. Houston, R.J. Badain, P. Troncosa, "Texture analysis of digitised prostate pathological cross-section", SPIE Proceedings of Medical Imaging: Image Processing, **1898**, 456-470, 1993.
 10. P.H. Bartels, T. Gahm, D. Thompson, "Automated microscopy in diagnostic histopathology: from image processing to automated reasoning", *International Journal of Image Systems and Technology*, **8**, 214-223, 1997.
 11. P.H. Bartels, H.G. Bartels, R. Montironi, P.W. Hamilton, D. Thompson, "Machine vision in the detection of prostate lesions in histologic sections", *Analytical and Quantitative Cytology and Histology*, **20**, pp. 358-364, 1998.
 12. P.H. Bartels, D. Thompson, R. Montironi, G. Mariuzzi, P.W. Hamilton, "Automated reasoning system in histopathologic diagnosis and prognosis of prostate cancer and its precursors", *European Urology*, **30**, 222-233, 1996.
 13. P.H. Bartels, D. Thompson, R. Montironi, "Knowledge-based image analysis in the precursors of prostatic adenocarcinoma", *European Urology*, vol. **30**, pp. 234-242, 1996.
 14. P.W. Hamilton, P.H. Bartels, R. Montironi, "Automated histometry in quantitative prostate pathology", *Analytical and Quantitative Cytology and Histology*, **20**, 443-460, 1998.
 15. U. Catalyurek, M.D. Beynon, C. Chang, T. Kurc, A. Sussman and J. Saltz, "The virtual microscope", Technical Report, CS-TR-4405 and UMIACS-TR-2002-85, University of Maryland, Department of Computer Science and UMIACS, Oct. 2002.
 16. A.R. Smith, "Color Gamut Transform Pairs", *Computer Graphics (SIGGRAPH '78 Proceedings)*, **12**, 12-19, 1978.
 17. D.S. Taubman, M.W. Marcellin, *JPEG2000: image compression fundamentals, standards, and practice*, Kluwer Academic Publishers, 2002.
 18. C. Christopoulos, A. Skodras and T. Ebrahimi, "The JPEG2000 still image coding system: an overview", *IEEE Trans. Consumer Electronics*, **46(4)**, 1103-1127, 2000.
 19. D.S. Taubman and M.W. Marcellin, "JPEG2000: standard for interactive imaging", Proceedings of the IEEE, **90(8)**, 1336-1357, 2002.

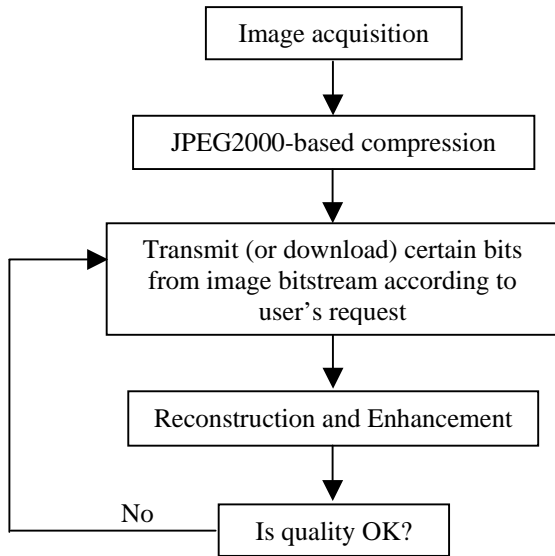


Fig. 1: Block diagram of the proposed computer aided diagnosis scheme

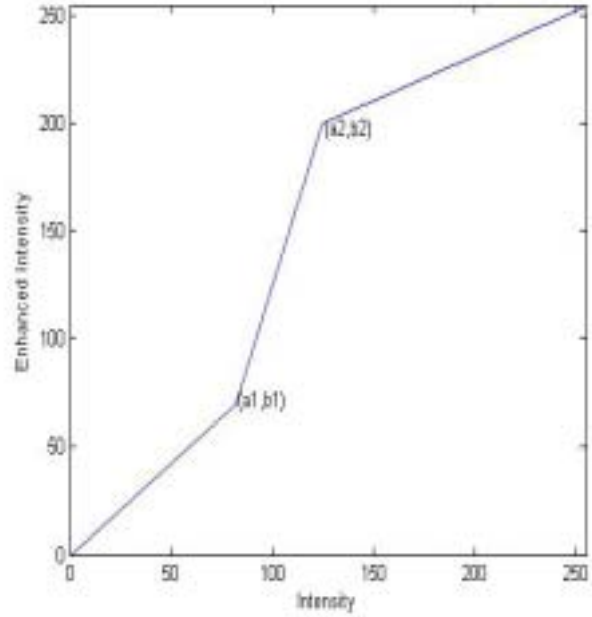


Fig. 2: Contrast enhancement function

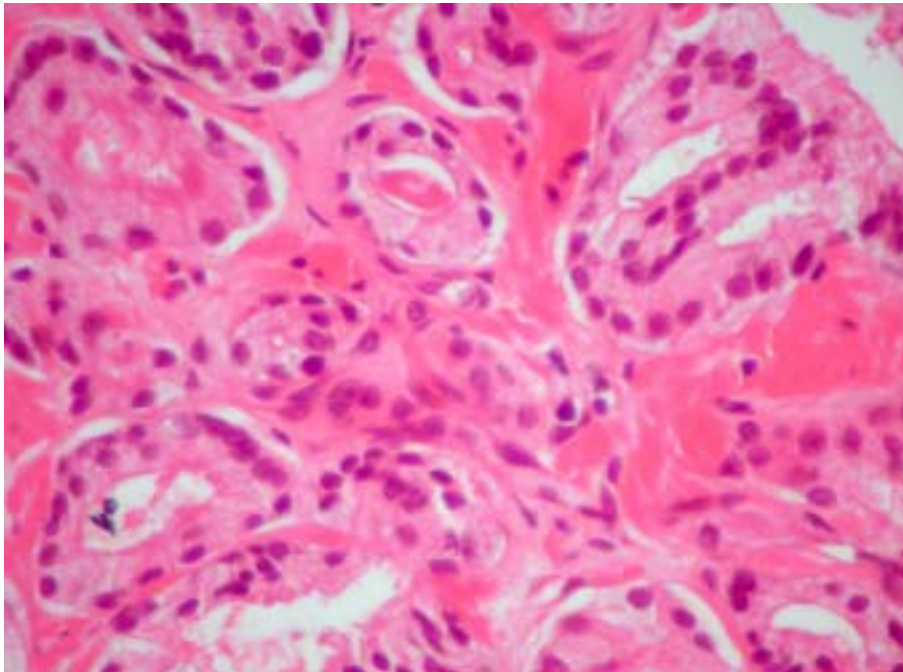


Fig. 3: The test image of prostate gland.

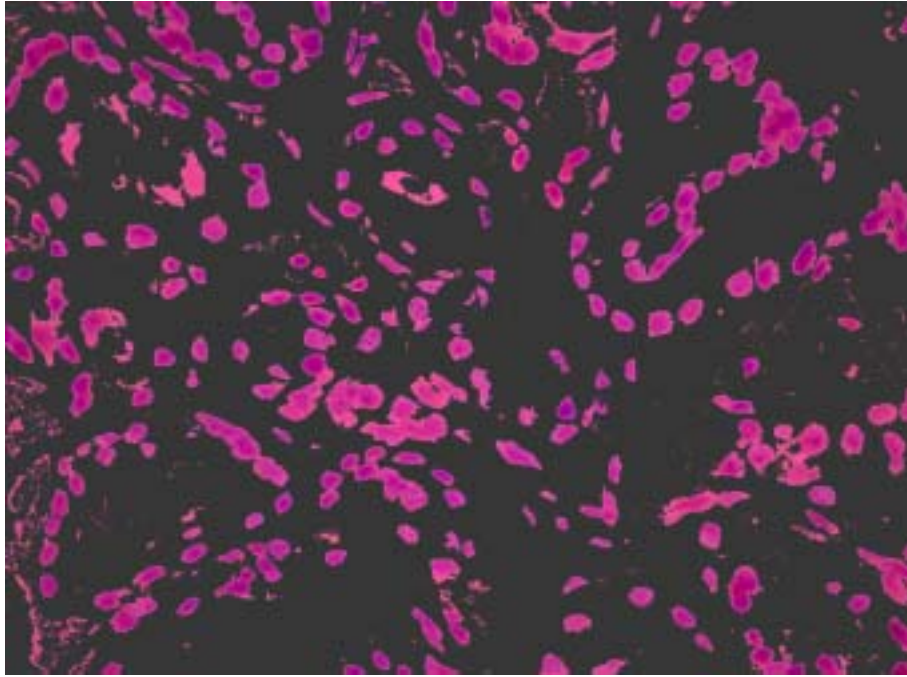


Fig. 4: Nuclei regions of the test images

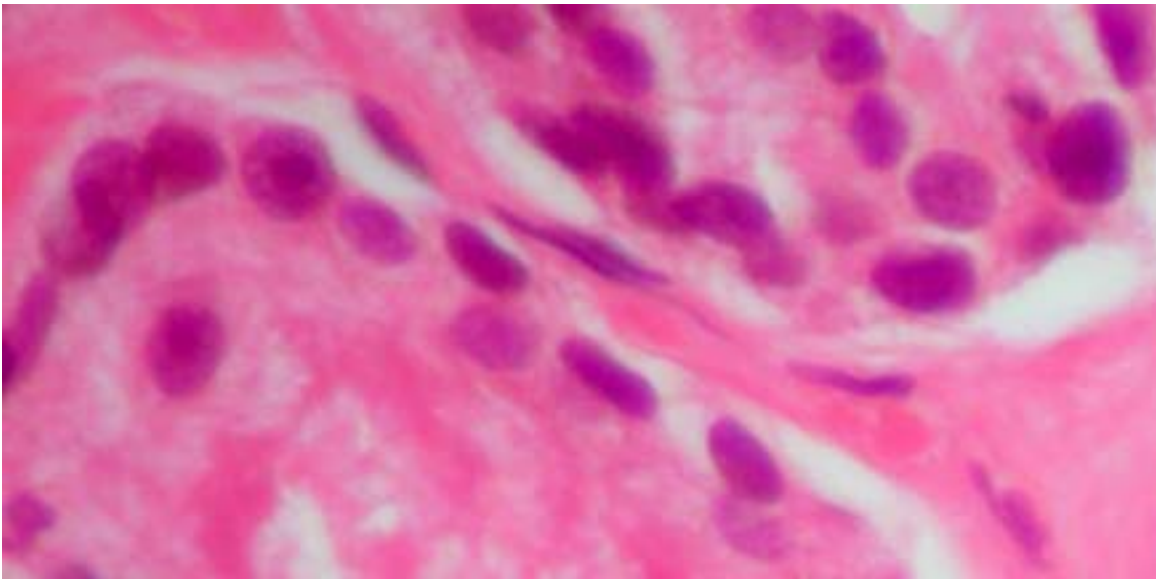


Fig. 5: Upper left portion of the test image, displayed at full resolution.

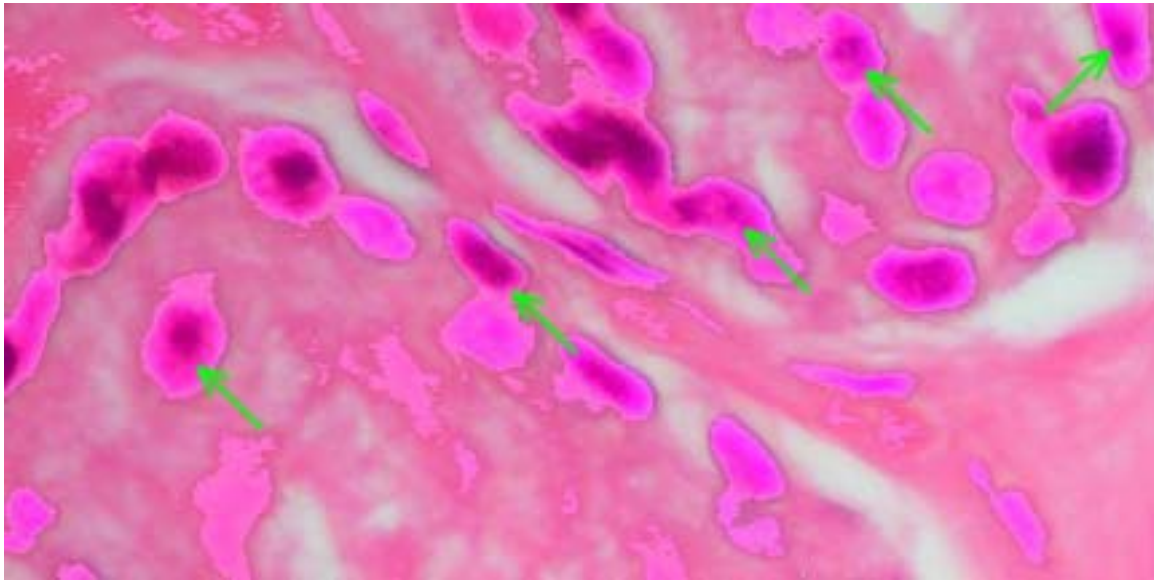


Fig. 6: Nuclei-enhanced version of the test image shown in Fig. 5. The arrows show the nucleoli that were not visible in the normal image.

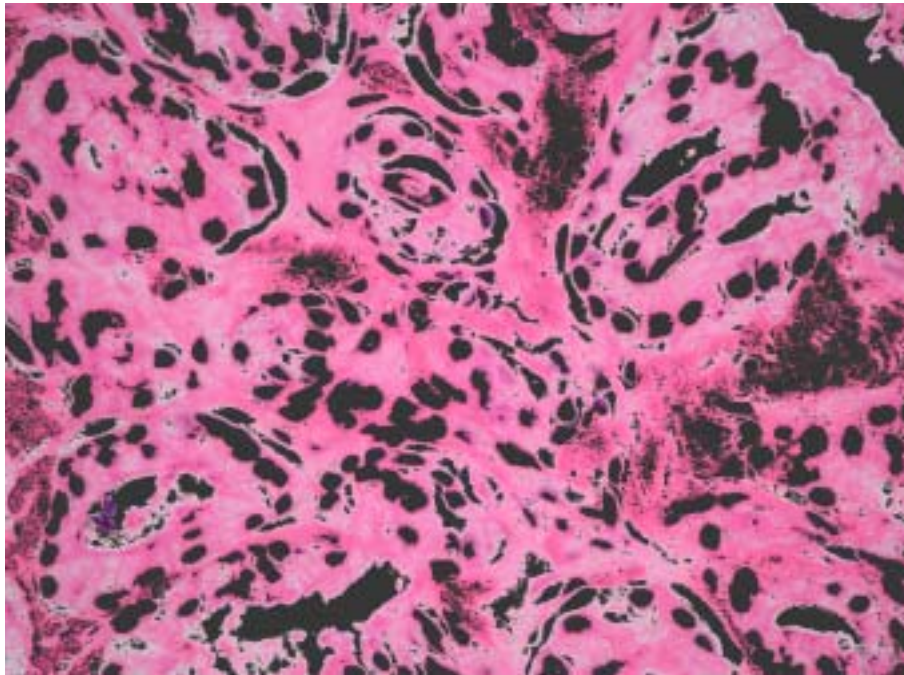


Fig. 7: Cytoplasm regions of the test image. This also contains some portions of stroma.

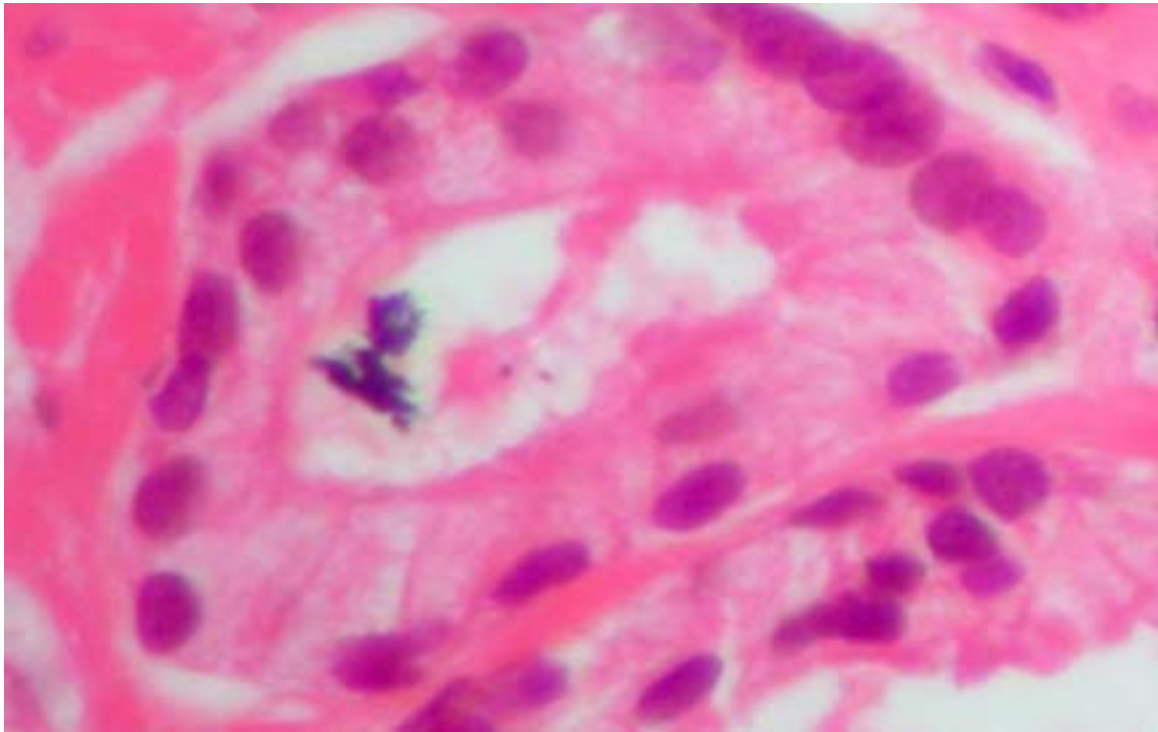


Fig. 8: Lower left portion of the test image, displayed at full resolution.

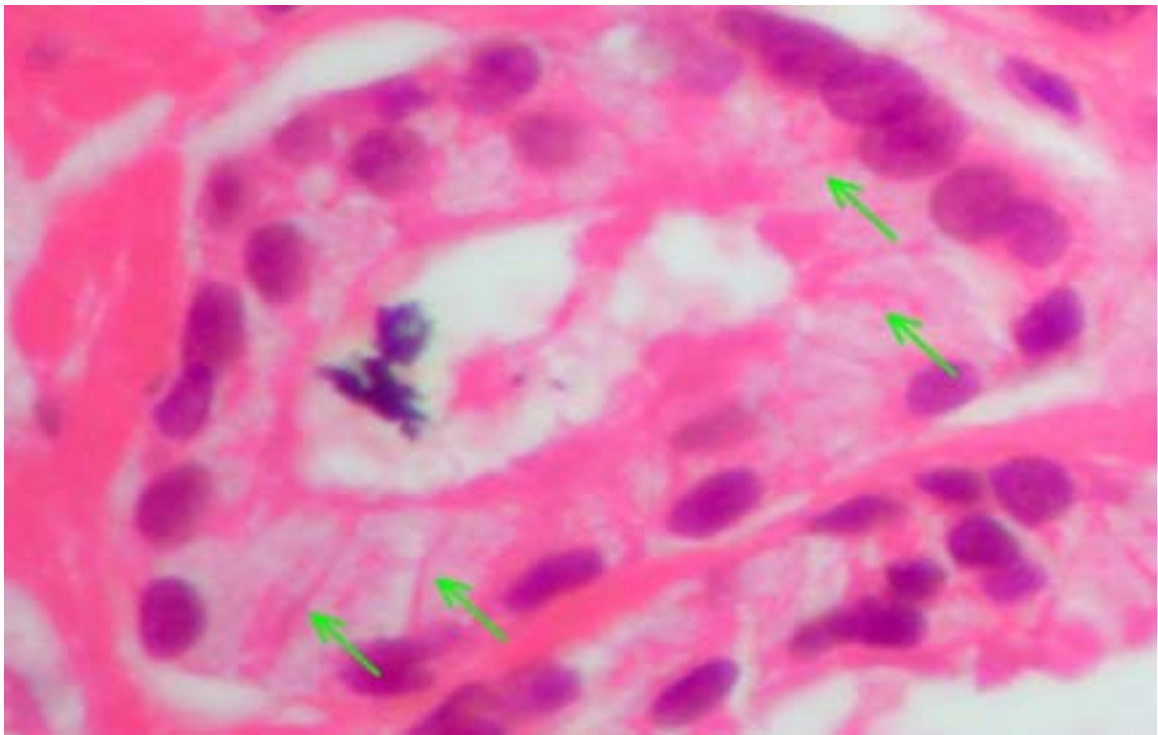


Fig. 9: Cytoplasm-enhanced version of the test image shown in Fig. 8. The arrows show the strengthened cell membranes.

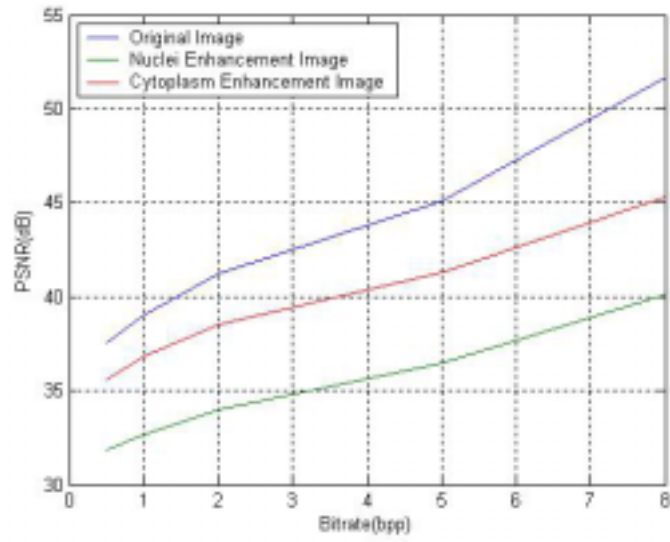


Fig. 10: Bit-rate vs. PSNR plots of compressed test image.

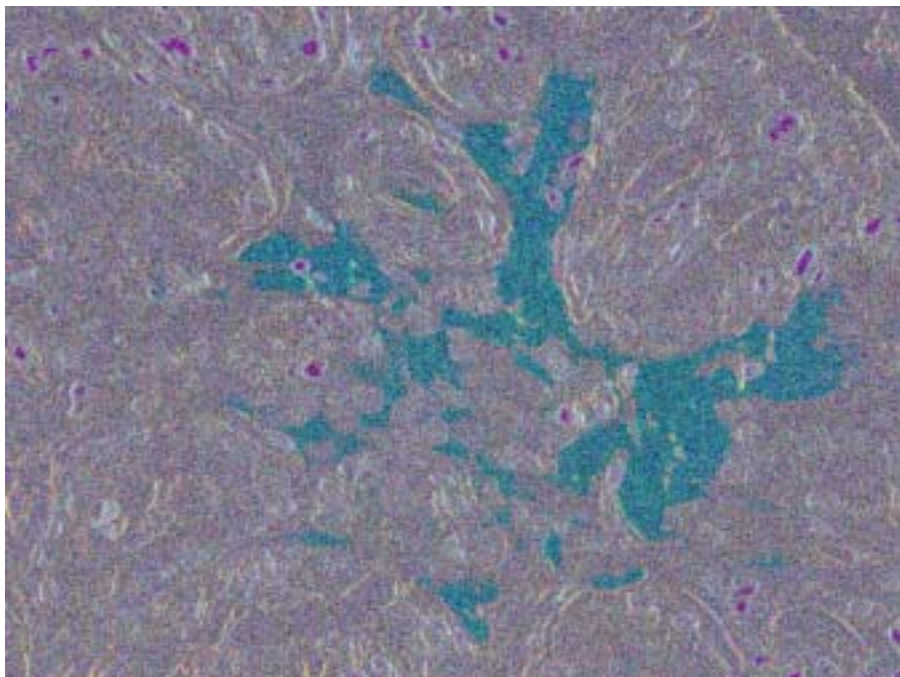


Fig. 11: The difference image of the original test image and its reconstructed image at 2 bpp.